Journal of Chromatography A, 1218 (2011) 4249–4256

Contents lists available at ScienceDirect

Journal of Chromatography A

journal homepage: www.elsevier.com/locate/chroma

Asymmetrical flow field-flow fractionation with multi-angle light scattering and quasi elastic light scattering for characterization of poly(ethyleneglycol-b-ε-caprolactone) block copolymer self-assemblies used as drug carriers for photodynamic therapy

Jérôme Ehrhart[a], Anne-Françoise Mingotaud[a], Frédéric Violleau[b,*]

[a] Université de Toulouse, UPS/CNRS, IMRCP, 118 route de Narbonne, F-31062 Toulouse Cedex 9, France
[b] Université de Toulouse, Ecole d'Ingénieurs de Purpan, Laboratoire d'Agro-Physiologie, UPSP/DGER 115, 75, voie du TOEC, BP 57611, F-31076 Toulouse Cedex 03, France

ARTICLE INFO

Article history:
Available online 22 January 2011

Keywords:
Asymmetrical flow field-flow fractionation
Static light scattering
Dynamic light scattering
Nanoparticles
Self-assembly
Drug delivery

ABSTRACT

Poly(ethyleneoxide-b-ε-caprolactone) (PEO-b-PCL) self-assemblies in water were characterized by asymmetrical flow field-flow fractionation (AsFlFFF), with on-line coupling with quasi-elastic light scattering (QELS), multi-angle light scattering (MALS), refractive index and UV/Vis detection. We report here the AsFlFFF analysis of three different nanoparticular self-assembled systems of PEO-PCL polymers in aqueous media, each polymer differing by the mass of the PEO and PCL fragments. Thus, self-assembled water samples of {PEO(2000)-b-PCL(2600)}, {PEO(5000)-b-PCL(1400)} and {PEO(5000)-b-PCL(4000)} were analyzed by AsFlFFF. In most cases, the size obtained by AsFlFFF was similar to the one characterized by DLS. However, in some instances, only AsFlFFF revealed the presence of several self-assemblies with very different sizes. These nanoparticles being used for the targeted delivery of photosensitizers in photodynamic therapy, it was important to fully characterize the samples in terms of size and size distribution, molecular weight, Ip, aggregation number and also to assess whether the photosensitizer was inside the nanoparticles. AsFlFFF proved to be a very efficient technique which enabled this study without any destruction of the nanoparticles.

1. Introduction

Design, synthesis, characterization and applications of nanoparticles (NPs) as nano-carriers for drugs, especially in the field of cancer therapy, are topics of interest in current nanomedicine, and remain a future fundamental and economical challenge [1,2]. This kind of approach, i.e. the use of nano-carriers entrapping active molecules, presents strong advantages such as improved therapeutic efficiency and selectivity for tumorous cells as well as to decrease the administered drug amount. This becomes possible owing to the enhanced permeation and retention effect (EPR), coming from local disjunction of blood vessels in the vicinity of a solid tumor associated with a very poor lymphatic system [3–5]. Thus, NPs with an optimal size of 10–100 nm, which can circulate long enough in blood without being detected by the immune system, will passively concentrate into the solid tumor. As a consequence, side effects are drastically decreased and the drug efficiency is increased.

Among all approaches to cancer treatment using drug delivery systems (magneto-therapy, hyperthermia, chemotherapy, radiotherapy), we are especially interested in using nano-carriers for photodynamic therapy (PDT) [6,7]. This method is based on the use of a photosensitizer (pstz), which gets distributed to the whole body and accumulates after several days into the tumor. During the subsequent step of irradiation, this pstz produces singlet oxygen species ($^1O_2$) which induce irreversible cell damages, leading to cell death.

The available commercial types of pstz (Photofrin™, Foscan™) are efficient but suffer from a poor selectivity for cancerous tissue. This implies the use of high doses of drugs, leading to severe side effects. Moreover, increasing the drug amount may lead to aggregation, owing to its porphyrin structure [8]. This is detrimental for PDT applications, since this leads to a strong decrease of the fluorescence quantum yield [9]. It is therefore necessary to develop new efficient nano-carriers enabling the encapsulation and transport of the pstz in the active monomeric form. These two major problems, i.e. poor selectivity for tumor and the presence of the inactive form of the pstz in aqueous media, could be overcome by the use of NPs like micelles or vesicles. Indeed, these possess a lipophilic part, potentially permitting the encapsulation of the pstz in its monomeric form, and a peripherical hydrophilic shell,

* Corresponding author. Tel.: +33 5 61 15 29 78.
E-mail address: frederic.violleau@purpan.fr (F. Violleau).

0021-9673/$ – see front matter © 2011 Elsevier B.V. All rights reserved.
doi:10.1016/j.chroma.2011.01.048

allowing the solubilization and transport of the [NP-pstz] system to the cancerous tissues.

Many biocompatible amphiphilic diblock copolymers have been widely used for more than fifteen years as drug nanocarriers [10–12]. These copolymers may form NPs in water, typically of a micelle or vesicle nature. For this purpose, we chose poly(ethyleneoxide-b-ε-caprolactone) block copolymers (PEO-PCL), which have already been used as nanovectors [13,14]. This type of copolymers presents several advantages for the use as nano-vector: they are biocompatible, biodegradable and their self-assembly in water gives rise to NPs with a size often below 200 nm [15–17], small enough to escape the immune system. This ensures a sustained blood circulation half-time, which is mandatory to benefit from EPR effect.

PEO-PCL is composed of two blocks, the PEO being hydrophilic, and the PCL hydrophobic. Depending on chain length, different self-assembled NPs of various types, shapes and sizes could possibly be obtained in aqueous media. In our project, the final goal is to establish correlation between shape, size, morphology, loading capacity and biological efficiency. For pharmaceutical application and transfer to the clinical level, the nano-carriers themselves have to be characterized as thoroughly as possible in terms of particle size distribution (PSD), size, morphology, aggregation number and polydispersity index (Ip), because nanoparticles ability to enter into cells, biological efficiency or sub-cellular location is closely related to these parameters [18,19].

For particle size determination, different characterization methods are commonly used, either in solution or not. Dynamic light scattering (DLS) analysis, also called QELS, is often used because it is fast, cheap and it requires limited sample manipulation since NPs can be analyzed in any dispersing medium. DLS measures the Stokes diffusion coefficient (D) of NPs in the dispersing medium, which is correlated to the NP hydrodynamic radius (Rh). Electron microscopy (SEM, TEM) and atomic force microscopy (AFM) are also widely used methods for size determination. The observation of samples in the dried state can give access to physicochemical parameters, including size, particle size distribution (PSD) and morphology [20–22]. In the case of PEO-PCL polymers, the observations often corroborated the results obtained with DLS but were found to be sometimes not reproducible, without any rational reason. Moreover, since the NPs are observed in dried condition, the observed size/morphology may differ from the native one.

Static multi angle light scattering (MALS) is another method for characterizing macromolecules or aggregates in solution and is based on the measurement of the angular dependence of the LS intensity. MALS detection gives information on the radius of gyration (Rg) and the aggregation number. Since the ratio Rg/Rh depends on NP shape and density distribution, MALS detection can also provide information on the NP conformation and internal structure. However, similarly to DLS, MALS relevance is reduced for samples with complex and multimodal PSD. Moreover, the Rg determination is sometimes difficult for particles having an Rg smaller than 10 nm.

For this reason, QELS and MALS analyses are complementary but could not properly be applied for a correct PSD determination of a complex NP sample. Using AsFlFFF to first separate possible multiple populations of nanoparticles before analysis appears to be a good strategy in order to obtain thorough information on the nano-objects present in solution.

Furthermore, the ability of a nanoparticular sample to encapsulate the photosensitizer has to be proven before determining the maximum loading capacity. The aim of this paper is to explain how asymmetrical flow field-flow fractionation (AsFlFFF), coupled with several detection systems, was found to be an efficient method to obtain these characterizations. This method has been already described in the literature for the analysis of various nanoparticular systems: metallic [23,24], aqueous C60 [25] or polymeric [26–28]. In some cases, the drug loading was successfully analyzed [29–31]. Only a few examples however have dealt with polymeric micelles [32].

In the work presented in this paper, self-assembled NP samples obtained from three different PEO-PCL polymers, each one differing by the size of each block, were used. Thus, self-assemblies in water of {PEO(2000)-b-PCL(2600)}, {PEO(5000)-b-PCL(1400)} and {PEO(5000)-b-PCL(4000)}, where the number in brackets represents the mass corresponding to the block, were analyzed, characterized and their ability to serve as nano-carriers was investigated. The pstz used in this study is Pheophorbide (a) (Pheo), which presents a high $^1O_2$ quantum yield (0.6).

2. Materials and methods

2.1. Chemicals

Poly(ethyleneoxide-b-ε-caprolactone) {PEO(2000)-b-PCL(2600)}, {PEO(5000)-b-PCL(1400)} and {PEO(5000)-b-PCL(4000)} were purchased from Gearing Scientific. Their purity and molar mass were checked by ^{1}H NMR and size exclusion chromatography. The solvents (from SDS) were used as received. Pheophorbide (a) (Pheo) was obtained from an already published protocol [33].

2.2. Formation of the empty nanoparticles

20 mg of poly-(ethyleneoxide-b-ε-caprolactone) were dissolved in 0.4 ml of acetone and the solution sonicated for 5 min. The polymer solution was added dropwise under stirring to 5 ml of ultrapure water filtered on 250 μm membrane. The solution was left standing for 2 days without stirring to enable solvent evaporation at room temperature.

2.3. Formation of the Pheophorbide (a) charged nanoparticles

For Pheophorbide (a) containing nanoparticles, two stock solutions of Pheophorbide (a) in acetone were prepared: the first one at a concentration of 2.17×10^{-6} M and the second one at 1.09×10^{-6} M.

Solutions at the ratios $n_{Pheo}/n_{polymer}$ 1/5, 1/10 and 1/20 were prepared by adding the necessary calculated volume of the 2.17×10^{-6} M stock solution to 20 mg of polymer and the volume was completed to 0.4 ml with acetone. The solutions at the ratios 1/30 and 1/50 were prepared in the same way by using the second stock solution of Pheo at 1.09×10^{-6} M. These solutions were then sonicated until the polymer dissolved. The prepared solutions were finally added dropwise under stirring to 5 ml of ultrapure water filtered on 250 μm membrane. The solutions were left standing for 2 days without stirring to enable solvent evaporation.

2.4. DLS

Dynamic light scattering was carried out at 25 °C on a Malvern Zetasizer NanoZS. Data were analyzed by the general purpose method, using non-negative least square (NNLS).

2.5. AsFlFFF-MALS-QELS

The asymmetrical flow field-flow fractionation instrument was an Eclipse 2 System (Wyatt Technology Europe, Dernbach, Germany). The AsFlFFF channel had a trapezoidal geometry where the length is 17.3 cm, with an initial breadth of 1.15 cm and final breadth of 0.2 cm. The accumulation wall was an ultrafiltration membrane of regenerated cellulose with 10 kDa cut-off (Wyatt Technology Europe, Dernbach, Germany). An Agilent 1100 Series

Isocratic Pump (Agilent Technologies, Waldbronn, Germany) with an in-line vacuum degasser and an Agilent 1100 Autosampler delivered the carrier flow and handled sample injection into the AsFlFFF channel. A 0.1 mm in-line filter (VVLP, Millipore, Germany) was installed between the pump and the AsFlFFF channel. The products were detected with a 18 angle multi-angle light scattering (MALS) DAWN-Heleos-II (Wyatt Technology, Santa Barbara, CA, US), an OptilaRex Refractometer (Wyatt Technology, Santa Barbara, CA, US), a UV detector Agilent 1100 (λ = 412 nm) and a QELS detector. The MALS detectors were normalized with bovine serum albumin (BSA). For the calibration of scattering intensity, filtered toluene (HPLC grade) was used. Water with 0.02% sodium azide filtered before use (vacuum filtration system using Gelman filters of 0.1 mm) was used as eluent. Two spacers were used. Channel thickness (w) calculated from retention time of BSA ($D = 6.11 \times 10^{-7}$ cm^2/s) and ferritin ($D = 4.10 \times 10^{-7}$ cm^2/s) were respectively 238 and 108 μm.

3. Theory

3.1. AsFlFFF

The underlying principles of AsFlFFF have been reviewed elsewhere [34–43]. AsFlFFF is a flow based method where the separation takes place in a narrow, open channel without any packing. A carrier liquid is continuously pumped through a channel from the inlet to the outlet establishing a parabolic flow profile.

One of the channel walls, called the accumulation wall, consists in a semi permeable cellulose membrane through which a part of the carrier liquid and objects with size under membrane cutoff are allowed to exit. The secondary flow is called the cross-flow. This movement is counteracted by the diffusion of the sample components. The net result is that the distance between the sample components and the accumulation wall depends on individual diffusion coefficient D (and thereby size) of the components. Due to the parabolic velocity profile of the main channel flow, the sample components elute from the channel at different retention times depending on their distance to the wall which depends on their size. Owing to the absence of any packing, a minimization of the interaction at the interfaces is obtained. This strongly decreases the risk of modifying the analyzed particle, therefore rendering AsFlFFF a more adequate technique than SEC in case of NP separation.

In normal mode flow field-flow fractionation, the retention time (t_r) of samples is related to diffusion of the particles according to a theory described elsewhere [34]. Consequently, the hydrodynamic diameter D_h is proportional to t_r and can be determined via Stokes–Einstein equation [35–39].

3.2. Static and dynamic light scattering

Theory and principles of static light scattering (MALS) can be found in literature [44,45]. In solution, macromolecules scatter light in all directions and the scattered intensity depends on many parameters, in particular the scattering angle, the molar mass and the radius of gyration [46]. These parameters can be calculated using Zimm diagram.

In quasi-elastic light scattering (QELS) or dynamic light scattering (DLS), time-dependent fluctuations in the scattered light signal are measured using a fast photon counter. The fluctuations are directly related to the rate of diffusion of the molecule in the solvent. The diffusion coefficient can be calculated from this correlation by different fitting methods. Therefore, the fluctuations can be analyzed to determine a hydrodynamic diameter (D_h) for the sample from the diffusion coefficient via Stokes–Einstein equation.

Table 1
Hydrodynamic diameters obtained by DLS.

	Average D_h (DLS)
{PEO(2000)-b-PCL(2600)}	17.7 ± 2 nm
{PEO(5000)-b-PCL(4000)}	18.2 ± 3 nm
{PEO(5000)-b-PCL(1400)}	84.4 ± 10 nm

4. Results and discussion

4.1. Analysis of the empty self-assembled NPs samples

4.1.1. Previous analysis

DLS analysis of the three polymer systems, i.e. {PEO(2000)-b-PCL(2600)}, {PEO(5000)-b-PCL(1400)}, {PEO(5000)-b-PCL(4000)}, gave reproducible results which are presented in Table 1. For all polymer samples, DLS data revealed a single population in number. Two size ranges of samples were identified: {PEO(2000)-b-PCL(2600)} and {PEO(5000)-b-PCL(4000)} led to nanoparticles with a hydrodynamic diameter close to 20 nm, whereas {PEO(5000)-b-PCL(1400)} gave 80 nm NPs. However, DLS gives no information on particle shape and morphology. Furthermore, in case of multimodal PSD, DLS measurements lead to results that do not reflect the reality in solution.

4.1.2. AsFlFFF analysis

As shown in Table 1, two size ranges of NPs were identified by previous DLS measurements on the native NP solutions of the three polymers. For this reason, it appeared difficult to separate and analyze both size ranges of samples under the same eluting conditions. Beside the choice of mobile phase, another parameter controlling the distribution of particles along the channel thickness (and therefore their separation) is the crossflow rate [34,47]. On one hand, a too low crossflow leads to no separation while a too high one leads to a very long separation time and could induce irreversible adsorption on the membrane [34]. The flow rates and the spacer thickness were thus chosen by taking into account these parameters to provide an optimal separation for each size range of NP samples.

4.1.2.1. AsFlFFF analysis of the small NPs samples. For the smallest NP samples obtained by self-assembly of {PEO(2000)-b-PCL(2600)} and {PEO(5000)-b-PCL(4000)}, a 238 μm spacer was found suitable. After preliminary trials with different flow rates, it was observed that the volumetric flow rate and consequently the linear flow velocity should be as low as possible to increase the residence time in the detector cell in order to get accurate QELS data. Thus, a 0.3 ml/min volumetric flow rate was selected for D_h calculation by the QELS data. Furthermore, increasing the injected quantity of materials had no effect on the accuracy of the D_h determination by QELS but caused an overloaded RI profile. Thereby, the results given thereafter were obtained with the eluting condition V_c = 0.4 ml/min, V_{out} = 0.3 ml/min, V = 10 μl, C = 4 mg/ml. We also noted that the gyration radius could not be accurately calculated, probably because NP size range was under 10 nm, close to the MALS detection limit.

The RI and QELS fractograms obtained with samples of {PEO(2000)-b-PCL(2600)} and {PEO(5000)-b-PCL(4000)} polymers are shown in Fig. 1.

As expected, for both samples, one major population of self-assembled NPs was identified, giving intense RI and QELS signals with RI peaks at 5.05 min and 6.87 min for {PEO(2000)-b-PCL(2600)} and {PEO(5000)-b-PCL(4000)} respectively. In addition, for both samples, a weak RI peak was also observed just after the void volume, which could be due either to smaller objects, or a portion of solubilized polymer in the case of {PEO(5000)-

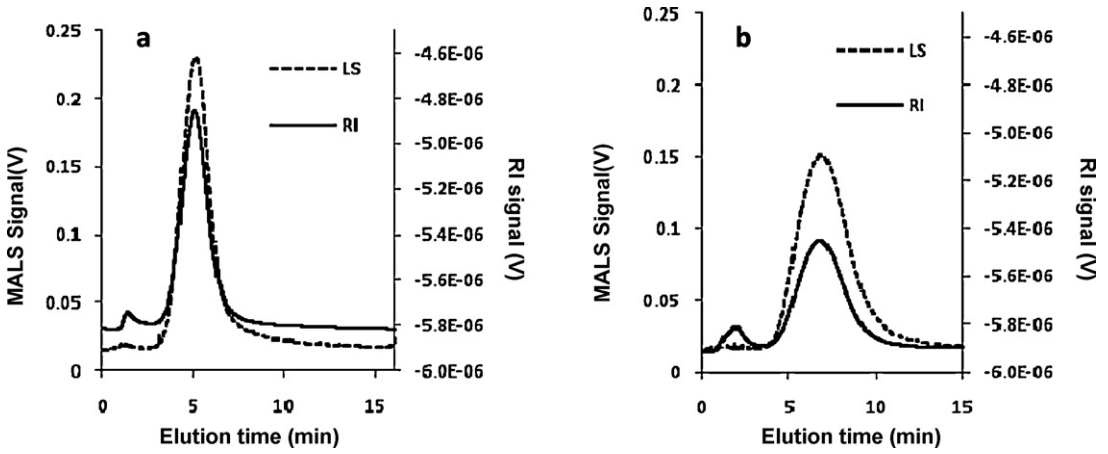

Fig. 1. Fractogram of (a) {PEO(2000)-b-PCL(2600)} and (b) PEO(5000)-b-PCL(4000)}. Conditions: V_{in} = 0.7 ml/min, V_{out} = 0.3 ml/min, V_c = 0.4 ml/min, channel thickness (w) = 238 μm.

b-PCL(4000)} whose molecular weight is close to the membrane cut-off. The hydrodynamic diameters calculated by the retention time (t_r) as a function of the quantitative signal for both systems are presented in Fig. 2.

The maximum RI intensities correspond to NPs with hydrodynamic diameters of 17.9 and 25.4 nm for the {PEO(2000)-b-PCL(2600)} and {PEO(5000)-b-PCL(4000)} systems respectively. It is noteworthy that the size distribution appeared narrower for the NPs resulting from the self-assembly of {PEO(2000)-b-PCL(2600)} since the D_h of the NPs was between 12 and 30 nm, while that of the NPs obtained with {PEO(5000)-b-PCL(4000)} was between 15 and 50 nm. In the same figure, the instantaneous molar mass is reported as a function of D_h. Molar masses of ca. 1.6×10^6 and 2×10^6 g mol^{-1} were determined for the {PEO(2000)-b-PCL(2600)} and {PEO(5000)-b-PCL(4000)} systems respectively at the maximum intensities of the quantitative signal.

Furthermore, to validate the D_h calculations based on the retention time (t_r), these were compared to the D_h calculated using QELS

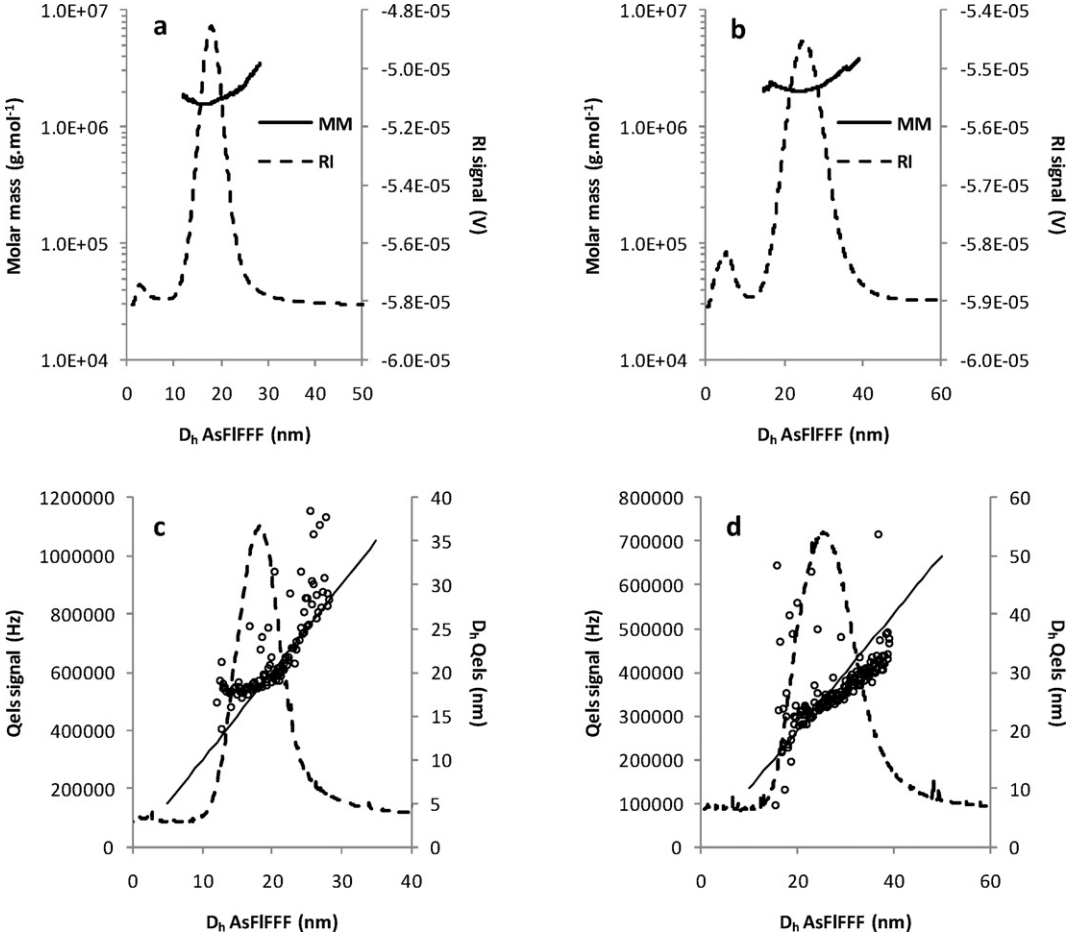

Fig. 2. Molar mass and RI signal as a function of D_h (t_r) for (a) {(PEO2000)-b-PCL(2600)}; (b) {(PEO5000)-b-PCL(4000)} and QELS signal and D_h (QELS) as a function of D_h (t_r) for (c) {PEO(2000)-b-PCL(2600)}; (d) {PEO(5000)-b-PCL(4000)}.

Table 2
Average size, molar mass, n_{agg} and Ip for {PEO(2000)-b-PCL(2600)} and {(PEO5000)-b-PCL(4000)}.

Polymer	D_h (nm) (QELS)	D_h (nm) (t_r)	M_n (g/mol)	M_w (g/mol)	n_{agg}	Ip
{PEO(2000)-b-PCL(2600)}	20.2 (13%)	19.5	1.69×10^6 (2%)	1.71×10^6 (2%)	367.4	1.013 (3%)
{PEO(5000)-b-PCL(4000)}	26.8 (21%)	26.7	2.19×10^6 (4%)	2.22×10^6 (4%)	246.7	1.014 (6%)

data. Fig. 2 also shows the D_h calculated by QELS data as a function of that calculated with the retention time for both polymers. A good correlation exists for both systems and a linear fit is obtained mostly in the main population, between 20 and 30 nm.

Average values of size, molar mass, as well as aggregation numbers and Ip, obtained by the calculations from QELS, MALS and RI data are summarized in Table 2 for both self-assembled NPs.

The average hydrodynamic diameters, calculated by the retention time and by QELS data are close, approximately 20 nm for {PEO(2000)-b-PCL(2600)} and 27 nm for {PEO(5000)-b-PCL(4000)}. Even if MALS data did not permit to calculate any gyration radius, number and weight average molar masses (M_n and M_w) could be determined with good accuracies of 2% and 4% for {PEO(2000)-b-PCL(2600)} and {PEO(5000)-b-PCL(4000)} respectively. These accurate molar masses enable a precise calculation of the Ips, which are close to 1 for both NPs, showing the monodisperse character of the NPs. The aggregation number (n_{agg}), which is the result of the ratio $M_n/M_{polymer}$, could also be evaluated and showed that both NPs were composed on average of ca. 370 polymer molecules for the {PEO(2000)-b-PCL(2600)} system and 250 polymer molecules for the {PEO(5000)-b-PCL(4000)}.

Even if the gyration radius (Rg) could not be obtained by SLS measurements to calculate the shape factor Rg/Rh, micellar systems are strongly expected for these self-assembled polymers based on the NP size and aggregation number.

Finally, these NPs samples obtained by self-assembly in water from polymer {PEO(2000)-b-PCL(2600)} and {PEO(5000)-b-PCL(4000)} appear to be monodisperse. Size calculation from DLS, online QELS and retention time approximately showed the same results for the hydrodynamic diameter. Because of these interesting characteristics, i.e. Ip, satisfying PSD and size, these self-assembled polymers appear to be good candidates as nano-carriers for biomedical applications. Therefore, in the second part of this work, the ability of these self-assembled polymer samples to entrap and transport a drug content will be investigated.

4.1.2.2. AsFlFFF analysis of the large NPs sample. For the elution of the {PEO(5000)-b-PCL(1400)} polymer sample, a 108 μm spacer was chosen. Because of the expected NP size, this spacer appeared to be ideal to elute this sample with an acceptable elution time. After many trials, the flow rates V_c = 1.2 ml/min and V_{out} = 0.9 ml/min were chosen as the best eluting conditions. The RI and QELS fractograms in the selected eluting conditions are illustrated in Fig. 3.

The fractograms showed a first intense RI peak, superimposed with a QELS signal, appearing just after the void volume and signaling the presence of a significant population of small objects. Even with a higher cross-flow, this RI signal always appeared after the void volume, which did not enable a correct size determination since the ratio t_r/t_0 was too small. This population could correspond to either a soluble part of the polymer since the PEO water soluble chain is much longer than the PCL chain or self-assemblies of a limited number of polymer chains. This information about the overall content of the sample is of the highest importance for the proposed PDT application and, among all methods that we used to characterize these self-assemblies, AsFlFFF was the only one pointing out this population. As explained previously, DLS or MALS methods, by themselves, are not accurate to detect populations of small objects

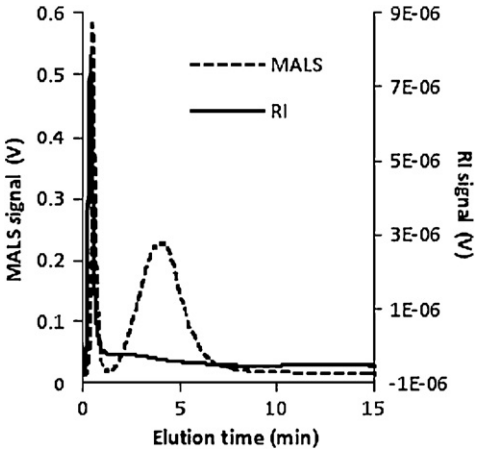

Fig. 3. Fractogram for {PEO(5000)-b-PCL(1400)}. Conditions: V_{in} = 2.1 ml/min, V_{out} = 0.9 ml/min, V_c = 1.2 ml/min, channel thickness (w) = 108 μm.

in a multimodal PSD. This is not the case by coupling these analysis methods and refractive index detection with AsFlFFF. Fractograms of the RI and QELS signals also revealed a second intense QELS signal with a maximum intensity at 4.01 min, superimposed with a small RI signal. The next calculations were made on these signals which correspond to the self-assembled polymer population.

Instantaneous molar mass and MALS signal have been traced as a function of the D_h calculated with the retention time (Fig. 4). A hydrodynamic diameter of 78.1 nm corresponded to the maximum QELS intensity. The size distribution appeared larger here since the hydrodynamic diameter of the NPs was between 25 and 140 nm. Concerning the instantaneous molar mass, a linear fit was observed with D_h between 50 and 100 nm with a molar mass of 8.9×10^7 g mol^{-1} determined at the maximum QELS intensity.

A gyration diameter could be obtained and its evolution as well as the evolutions of D_h calculated by QELS data and retention time are shown in Fig. 5. A good correlation between D_g and D_h calculated

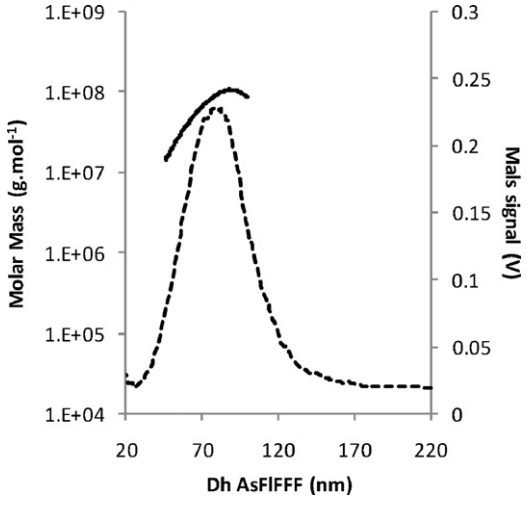

Fig. 4. MALS signal and D_h (QELS) as a function of D_h (t_r) for {PEO(5000)-b-PCL(1400)}.

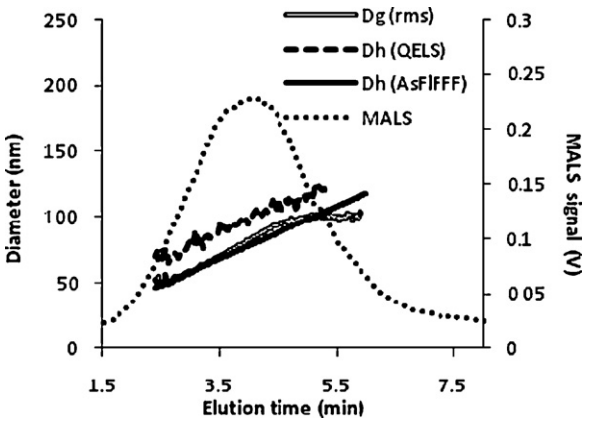

Fig. 5. Evolutions of D_g, D_h (QELS) and D_h (AsFlFFF) as a function of time.

by retention time was observed and the D_h calculated by QELS data also showed a linear evolution but at slightly larger sizes.

Average size values, molar mass as well as aggregation number and Ip, obtained by the calculations from QELS, MALS and RI data are summarized in Table 3.

As expected, the average D_h calculated with the retention time and QELS data are quite close, 77.1 and 85 nm respectively which is a strong argument for the validity of the analysis. Previous DLS measurements (see Table 1) also showed the same NP size. A D_g of 76.2 nm was also obtained with a good accuracy using MALS data. Moreover, the D_g/D_h shape factor was found between 0.90 and 0.99, a sign that nanoparticles were spherical and empty, which is characteristic of a vesicular structure. This result was expected in regards to the NPs and polymer sizes. Values of M_n and M_w were also calculated with an accuracy better than 1%. This allowed a precise Ip determination at 1.40, indicating the polydisperse character of the NPs population. Furthermore, the number of aggregation, calculated with M_n, indicated that a NP was composed of ca. 6700 polymer molecules.

Finally, this self-assembled NP sample of {PEO(5000)-b-PCL(1400)} could not be properly used as nano-carriers for application in PDT since the sample contains a significant population of the solubilized form of the polymer and the NPs population presents a too high polydispersity.

4.2. AsFlFFF analysis of the Pheo charged NPs samples

For efficient nanocarriers, a good interaction between the NP and the drug should exist to maintain the drug content within the NP during the transport in blood. Separation analysis like AsFlFFF, where the nano-carriers and their content are transported from a point to another under a double flow is in this case particularly suitable because conditions of pressure and flow could be assimilated to a simplistic mimicking of the blood flow. Thus, an outlet optic detection ($\lambda = 412$ nm) was added to the other detectors to evaluate the ability of the previously selected NPs samples ({PEO(2000)-b-PCL(2600)} and {PEO(5000)-b-PCL(4000)}) to entrap and transport Pheo. This wavelength was chosen because of the intense extinction coefficient of Pheo at 412 nm ($\approx 100\,000\ mol^{-1}\,l\,cm^{-1}$).

For this purpose, different solutions of each self-assembled polymer with increased concentrations of Pheo were submitted to the AsFlFFF analysis. Ratios ($n_{Pheo}/n_{polymer}$) of 1/50, 1/30, 1/20, 1/10, 1/5 and 1/2 were used for both systems. By this way it is possible to determine the presence of Pheo within the NP and the maximum loading capacity of both systems. The same eluting conditions as before were used ($V_c = 0.4$ ml/min, $V_{out} = 0.3$ ml/min, $V = 10$ μl). Because Pheo was the only chromophore absorbing at this wavelength and because the particles themselves led to a slight baseline increase owing to turbidity, the UV fractograms were substracted from the UV fractogram obtained with the empty NP samples.

The RI and UV fractograms obtained for {PEO(2000)-b-PCL(2600)} and {PEO(5000)-b-PCL(4000)} with various quantities of Pheo are presented in Fig. 6. These RI fractograms demonstrated that the same quantity of material was injected and analyzed since integration of the RI signals for a same system with various quantities of Pheo were really close. Furthermore, increasing the drug concentration did not lead to a significant increase of the NP size, since no evolution of the retention time was observed.

The UV fractograms obtained at different ratios $n_{Pheo}/n_{polymer}$ are also shown in Fig. 6 for both systems. UV signals increase with increasing ratio $n_{Pheo}/n_{polymer}$, which is consistent with increasing quantities of Pheo in the nanoparticle. Furthermore, the absorption peak is observed exactly at the same elution time as for the NPs, demonstrating the encapsulation of Pheo within the NP.

Because the environment and the aggregation state of Pheo could change the absorption spectrum and thus the absorption coefficient at 412 nm, the exact calculation of the quantity of Pheo within the NPs was not scientifically relevant. For this reason, the UV signals were only further used to evaluate the maximum loading capacity of each system. This was performed by tracing the evolution of the area of the absorption signal as a function of the ratio $n_{Pheo}/n_{polymer}$, as shown in Fig. 6. For the {PEO(2000)-b-PCL(2600)} system, a perfectly linear fit was observed between the surface area and the ratio employed until 0.1, which means that the particle entraped a quantity of Pheo proportional to the quantity of Pheo in solution. Beyond this point, the signal tended towards a plateau. This shows that a reasonable maximum loading capacity was obtained for $n_{Pheo}/n_{polymer}$ of 0.1.

In the same way, for {PEO(5000)-b-PCL(4000)}, the maximum loading capacity is obtained for the ratio $n_{Pheo}/n_{polymer}$ of 0.2, since a linear fit is observed between the integrated UV signal and the ratio until this point.

Even if the {PEO(5000)-b-PCL(4000)} system entraped Pheo with a higher ratio $n_{Pheo}/n_{polymer}$ than the {PEO(2000)-b-PCL(2600)} one, the calculated ratio $m_{pheo}/m_{polymer}$ appeared the

Table 3
Average sizes, shape factors, molar mass, n_{agg} and Ip for {PEO(5000)-b-PCL(1400)}.

Polymer	D_h (nm) (QELS)	D_h (nm) (t_r)	D_g (nm)	D_g/D_h (QELS)	D_g/D_h (t_r)	M_n (g/mol)	M_w (g/mol)	Ip	n_{agg}
{PEO(5000)-b-PCL(1400)}	85.0 (2%)	77.1	76.2 (2%)	0.9	0.99	4.31×10^7 (0.70%)	6.05×10^7 (0.60%)	1.40 (0.9%)	6739.1

Table 4
Calculation of the % weight of Pheo.

	Max ratio $n_{pheo}/n_{polymer}$	$m_{pheo}/m_{pheo} + m_{polymer}$ %weight	Number of pheo/NP = $n_{aggreg} \times$ Max ratio
{PEO(2000)b-PCL(2600)}	0.1	1.27	$367.4 \times 0.1 = 36.7$
{PEO(5000)-b-PCL(4000)}	0.2	1.30	$246.7 \times 0.2 = 49.3$

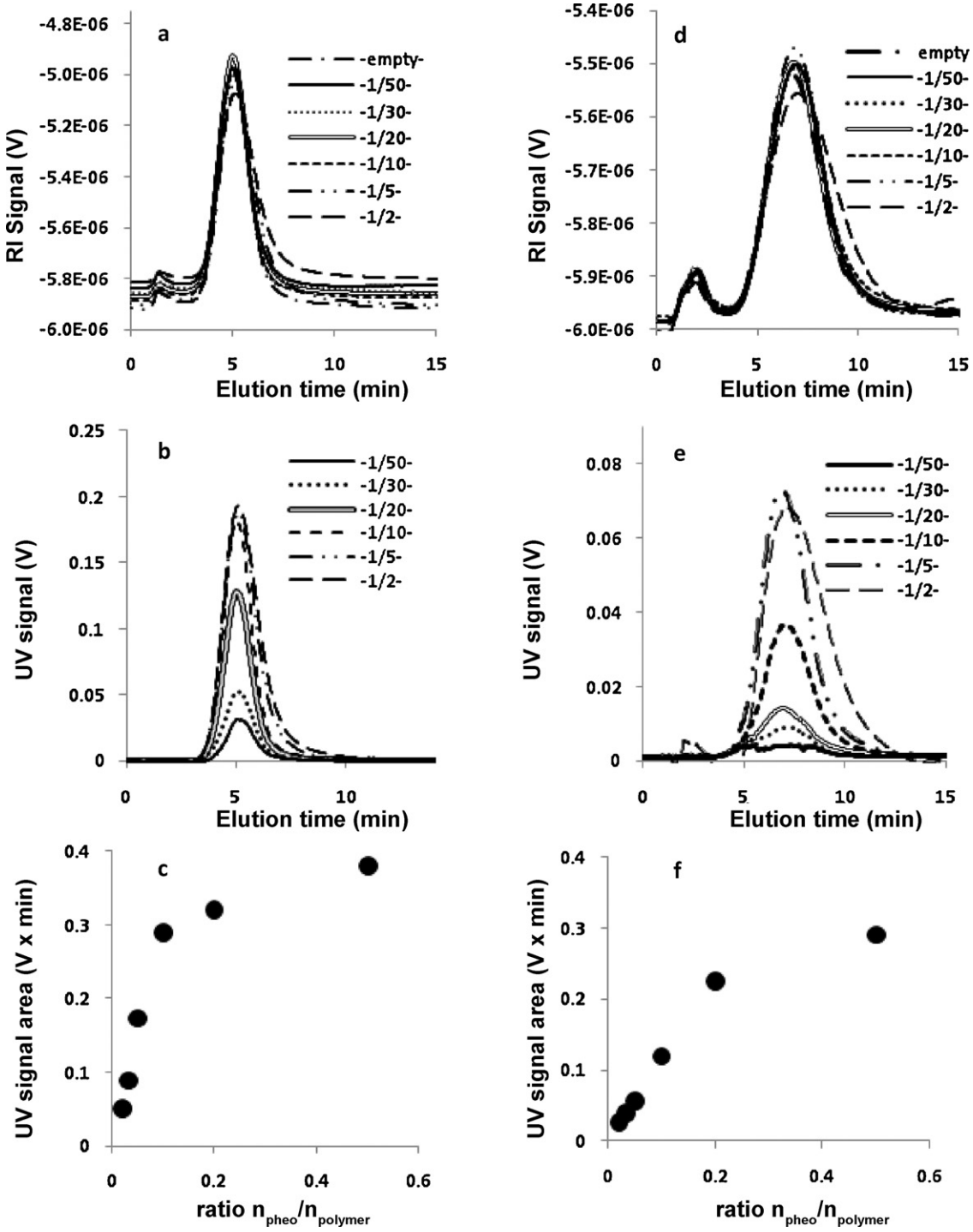

Fig. 6. Fractograms obtained with different quantites of Pheo for {PEO(2000)-b-PCL(2600)}: (a) RI signal; (b) UV signal (λ = 412 nm) and {PEO(5000)-b-PCL(4000)}; (d) RI signal; (e) UV signal (λ = 412 nm) and UV signal area as a function of the ratio $n_{Pheo}/n_{polymer}$ for (c) {PEO(2000)b-PCL(2600)}; (f) {PEO(5000)-b-PCL(4000)}. Conditions: V_{in} = 0.7 ml/min, V_{out} = 0.3 ml/min, V_c = 0.4 ml/min, channel thickness (w) = 238 μm.

same (≈1.3%) since this polymer is twice heavier than {PEO(2000)-b-PCL(2600)} (Table 4). Assuming that all the materials are eluted and detected without going through the membrane, the values of $n_{Pheo}/n_{polymer}$, % weight of Pheo ($m_{pheo}/m_{polymer}$) and number of pheo by NP are summarized in Table 4. The values of Pheo per NP are maximum ones, since it cannot totally be ruled out that some pheophorbide may not be incorporated in the nanoparticles. However, we were able to observe that, when doing dialysis, those Pheo molecules did not cross cellulose membranes.

5. Conclusion

AsFlFFF was found to be a very efficient soft separation method to finely analyze the NP samples. One of the major advantages of AsFlFFF lies in its ability in separating self-assembled polymer samples without any structure breakdown and its coupling with various detectors, enabling complementary information about the NP itself as well as its drug content in a single experiment.

Hydrodynamic diameters calculated with AsFlFFF analysis on our NP samples showed, for all investigated systems, a good

correlation with previous analyses made by DLS, but much finer information about samples contents as well as information about shape and morphology were obtained, especially for the {PEO(5000)-b-PCL(1400)} sample. For this, the gyration radius was determined by MALS data with a good accuracy and compared to the hydrodynamic diameters obtained by QELS data and retention time. This revealed that the NPs are vesicles since shape factors are close to 1. Furthermore, AsFlFFF revealed a very important population of possible soluble polymer in this sample, which is detrimental for the considered pharmaceutical application.

For {PEO(2000)-b-PCL(2600)} and {(PEO5000)-b-PCL(4000)} systems, AsFlFFF revealed that their Ip was close to 1 and that the PSD and sizes are suitable for their use as nano-carriers for application in PDT. In addition, the obtained results concerning the hydrodynamic diameters determined by retention time and QELS data are in good correlation with the ones obtained by DLS. Finally, the ability of these self-assembled NPs to encapsulate and transport Pheo has also been proven by AsFlFFF coupled additionally with absorbance detection. This also leads to the determination of the maximum loading capacity in the same experiment, without having to destroy the NP.

Acknowledgements

We would like to thank Wyatt Technology France for their assistance and Mireille Gaucher-Delmas for the technical support. This investigation was conducted with the financial support of ANR (French National Research Agency; project P3N COPODT).

References

[1] K. Riehemann, S.W. Schneider, T.A. Luger, G. Biana, M. Ferrari, H. Fuchs, Angew. Chem. Int. Ed. 48 (2009) 872.
[2] D. Peer, J.M. Karp, S. Hong, O.C. Farokhhzad, R. Margalit, R. Langer, Nat. Nanotechnol. 2 (2007) 751.
[3] Y. Matsumura, H. Maeda, Cancer Res. 46 (1986) 6387.
[4] P. Couvreur, C. Vauthier, Pharm. Res. 23 (2006) 1417.
[5] M.J. Alonso, Biomed. Pharmacother. 58 (2004) 168.
[6] B.W. Henderson, Photochem. Photobiol. 55 (1992) 145.
[7] K. Knop, A.F. Mingotaud, F. Violleau, N. El-Akra, J.-P. Souchard, Photochem. Photobiol. Sci. 8 (2009) 396.
[8] I. Eichwurzel, H. Stiel, B. Röder, J. Photochem. Photobiol. B 54 (2000) 194.
[9] B. Roeder, T.H. Hanke, S. Oelockers, C. Hackbarth, C. Symietz, J. Porphyrins Pthalocyanines 4 (2000) 37.
[10] J. Kreuter, in: H.S. Nalwa (Ed.), Encyclopedia of Nanoscience and Nanotechnology, American Scientific Publishers/Stevenson Ranch, California, 2004, p. 161.
[11] K. Kataoka, A. Harada, Y. Nagasaki, Adv. Drug Deliv. Rev. 47 (2001) 113.
[12] N. Nishiyama, K. Kataoka, Pharmacol. Ther. 112 (2006) 630.
[13] B. Li, E.H. Moriyama, F. Li, M.T. Jarvi, C. Allen, B.C. Wilson, Photochem. Photobiol. 83 (2007) 1505.
[14] J.-W. Hofman, M.G. Carstens, F. van Zeeland, C. Helwig, F.M. Flesh, W.E. Hennink, C.F. van Nostrum, Pharm. Res. 25 (2008) 2065.
[15] C. Allen, Y. Yu, D. Maysinger, A. Eisenberg, Bioconjug. Chem. 9 (1998) 564.
[16] S.Y. Kim, I.L. Shin, Y.M. Lee, C.S. Cho, Y.K. Sung, J. Control. Release 51 (1998) 13.
[17] X. Shuai, H. Ai, N. Nasongkla, S. Kim, J. Gao, J. Control. Release 98 (2004) 415.
[18] A. Verma, O. Uzuri, Y. Hu, H.S. Han, N. Watson, S. Chen, D.J. Irvine, F. Stellacci, Nat. Mater. 7 (2008) 588.
[19] S.E. Gratton, P.A. Ropp, P.D. Pohlaus, J.C. Luft, V.J. Madden, M.E. Napier, J.M. DeSimone, Proc. Natl. Acad. Sci. U.S.A. 105 (2008) 11613.
[20] H. Cohen, R.J. Levy, J. Gao, I. Fishbein, V. Kousaev, S. Sosnovsky, S. Slomkowsky, G. Golomb, Gene Ther. 7 (2000) 1896.
[21] R. Gref, A. Domb, P. Qellec, T. Blunk, R.H. Mueller, J.M. Verbavatz, R. Langer, Adv. Drug Deliv. Rev. 16 (1995) 215.
[22] L. Mu, S.S. Feng, J. Control. Release 86 (2003) 33.
[23] T. Joon Cho, V.A. Hackley, Anal. Bioanal. Chem. 398 (2010) 2003.
[24] A. Zattoni, D.C. Rambaldi, P. Reschiglian, M. Melucci, S. Krol, A.M. Coto Garcia, A. Sanz-Medel, D. Roessner, C. Johann, J. Chromatogr. A 1216 (2009) 9106.
[25] C.W. Isaacson, D. Bouchard, J. Chromatogr. A 1217 (2010) 1506.
[26] J.C. Zillies, K. Zwiorek, G. Winter, C. Coester, Anal. Chem. 79 (2007) 4574.
[27] M.H. Smith, A.B. South, J.C. Gaulding, L.A. Lyon, Anal. Chem. 82 (2010) 523.
[28] P. Lian Ma, M.D. Buschmann, F.M. Winnik, Biomacromolecules 11 (2010) 549.
[29] W. Fraunhofer, G. Winter, C. Coester, Anal. Chem. 76 (2004) 1909.
[30] J. Kanzer, S. Hupfeld, T. Vasskog, I. Tho, P. Hölig, M. Mägerlein, G. Fricker, M. Brandl, J. Pharm. Biomed. Anal. 53 (2010) 359.
[31] D.Y. Kang, M.J. Kim, S.T. Kim, K.S. Oh, S.H. Yuk, S. Lee, Anal. Bioanal. Chem. 390 (2008) 2183.
[32] K. Loos, A. Böker, H. Zettl, M. Zhang, G. Krausch, A.H.E. Müller, Macromolecules 38 (2005) 873.
[33] K.W. Smith, D.A. Goff, D.J. Simpson, J. Am. Chem. Soc. 107 (1985) 4946.
[34] K.G. Wahlund, M.E. Schimpf, K.D. Caldwell, J.C. Giddings, Field-Flow Fractionation Handbook, Wiley Interscience, New York, 2000.
[35] B. Wittgren, K.G. Wahlund, H. Derand, B. Wesslen, Macromolecules 29 (1996) 268.
[36] G. Yohannes, S.K. Wiedmer, E.K.J. Tuominen, P.K.J. Kinnunen, M.L. Riekkola, Anal. Bioanal. Chem. 380 (2004) 757.
[37] G. Yohannes, J. Shan, M. Jussila, M. Nuopponen, H. Tenhu, M.L. Riekkola, J. Sep. Sci. 28 (2005) 435.
[38] G. Yohannes, S.K. Wiedmer, M. Jussila, M.L. Riekkola, Chromatographia 61 (2005) 359.
[39] G. Yohannes, S. Holappa, S.K. Wiedmer, T. Andersson, H. Tenhu, M.L. Riekkola, Anal. Chim. Acta 542 (2005) 222.
[40] J. Janča, in: E. Heftmann (Ed.), Chromatography: Fundamentals and Applications of Chromatography and Related Differential Migration Methods. Part A. Fundamentals and Techniques, 5th ed., 1992, p. 449.
[41] K.J. Wahlund, J.C. Giddings, Anal. Chem. 59 (1987) 1332.
[42] K.G. Wahlund, A. Litzén, J. Chromatogr. 461 (1989) 73.
[43] A. Litzén, K.G. Wahlund, Anal. Chem. 63 (1991) 1001.
[44] P. Wyatt, Anal. Chim. Acta 272 (1) (1993) 1.
[45] B.J. Zimm, J. Chem. Phys. 16 (12) (1948) 1093.
[46] M. Andersson, B. Wittgren, K.G. Wahlund, Anal. Chem. 73 (20) (2001) 4852.
[47] R.L. Hartmann, S. Kim Ratanathanawongs Williams, J. Membr. Sci. 209 (2002) 93.